Carrier generation and transport properties of heavily Nb-doped anatase TiO_2 epitaxial films at high temperatures

Daisuke Kurita, Shingo Ohta, and Kenji Sugiura
Graduate School of Engineering, Nagoya University, Furo-cho, Chikusa, Nagoya 464-8603, Japan

Hiromichi Ohta and Kunihito Koumoto[a)]
Graduate School of Engineering, Nagoya University, Furo-cho, Chikusa, Nagoya 464-8603, Japan and CREST-JST, Kawaguchi Center Building, 4-1-8 Honcho, Kawaguchi 332-0012, Japan

(Received 22 June 2006; accepted 12 August 2006; published online 7 November 2006)

To compare the intrinsic thermoelectric (TE) properties of heavily Nb-doped TiO_2 to those of heavily Nb-doped $SrTiO_3$ [S. Ohta *et al.*, Appl. Phys. Lett. **87**, 092108 (2005)], the electrical conductivity (σ), carrier concentration (n_e), Hall mobility (μ_{Hall}), and Seebeck coefficient (S) of heavily Nb-doped TiO_2 (anatase) epitaxial films were measured at high temperatures (300–900 K). The epitaxial films were grown on the (100)-face of $LaAlO_3$ single-crystalline substrates by a pulsed-laser deposition technique at 800 °C. The carrier effective mass (m^*) of the anatase TiO_2 epitaxial films was $\sim 1m_0$, which is an order of magnitude smaller than that of Nb-doped $SrTiO_3$ ($\sim 10m_0$). The estimated TE power factor ($S^2\sigma$) of the ~2%-Nb-doped anatase TiO_2 film ($n_e \sim 5 \times 10^{20}$ cm^{-3}) was $\sim 2.5 \times 10^{-4}$ W m^{-1} K^{-2} at 900 K, which is approximately 15% of the 20%-Nb-doped $SrTiO_3$ (1.5×10^{-3} W m^{-1} K^{-2}). The present findings will help establish a future TE material design concept for Ti-based metal oxides. © *2006 American Institute of Physics*. [DOI: 10.1063/1.2362990]

Thermoelectric energy conversion is one of the cleanest and environmentally compatible power generation technologies because unused heat sources are readily available, e.g., electric power plants, factories, automobiles, and computers, and can be directly converted into electric power by utilizing the Seebeck effect of a thermoelectric (TE) material.[1] Generally, TE materials are evaluated in terms of the following figure of merit, $ZT = S^2\sigma T\kappa^{-1}$, where Z, T, S, σ and κ are the figure of merit, the absolute temperature, the Seebeck coefficient, the electrical conductivity, and the thermal conductivity, respectively. ZT corresponds to the energy conversion efficiency of a Carnot cycle.

Recently, several metal oxides, including Nb-doped $SrTiO_3$ ($SrTi_{0.8}Nb_{0.2}O_3$, $ZT_{300\ K} \sim 0.08$, $ZT_{1000\ K} = 0.37$),[2–4] $Na_{0.7}CoO_2$ ($ZT_{300\ K} \sim 0.1$),[5] and $Ca_3Co_4O_9$ ($ZT_{300\ K} \sim 0.08$, $ZT_{1000\ K} \sim 0.3$),[6] exhibit a rather high ZT. These metal oxides have attracted growing attention as sources to generate thermoelectric power at high temperatures because they have potential advantages over state-of-the-art, high temperature thermoelectric materials, including a SiGe-based alloy ($ZT \sim 1$)[7] and β-$FeSi_2$ ($ZT \sim 0.3$),[8] in terms of chemical and thermal resistances at high temperatures (~1000 K). One of the most important features of these metal oxides as TE materials is the rather large Seebeck coefficient ($|S|$) even in a heavily carrier doped state.

Recently, we have reported that the ZT value of heavily Nb-doped $SrTiO_3$ increases with Nb content and reaches $ZT_{1000\ K} = 0.37$[2] at a 20%-Nb-doped state ($n_e = 4 \times 10^{21}$ cm^{-3}) because both the carrier concentration and the carrier effective mass (m^*) value of the conduction band bottom of $SrTiO_3$, which is composed of degenerated Ti $3d$-t_{2g} orbitals in the TiO_6 octahedral crystal field, increase with Nb content. Figure 1 schematically shows TiO_6 octahedra of (a) $SrTiO_3$ (perovskite structure, cubic, $a = 0.3905$ nm)[9] and (b) TiO_2 (anatase, tetragonal, $a = 0.3785$ nm, $c = 0.9513$ nm)[10], a major constituent of $SrTiO_3$, and the cor-

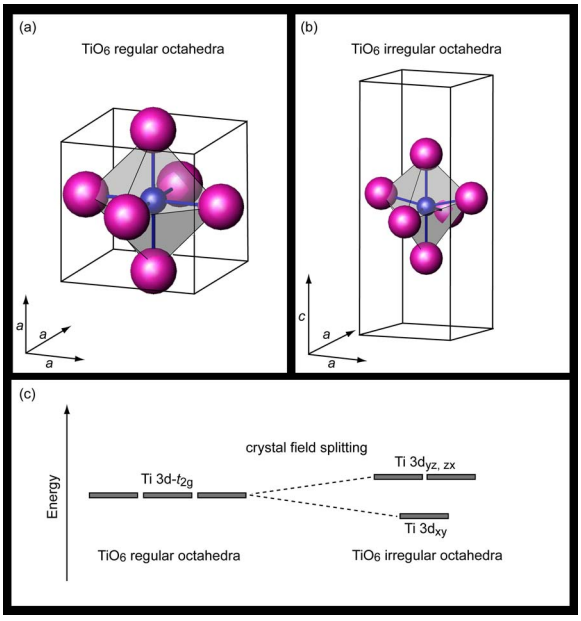

FIG. 1. (Color online) Schematic representation of TiO_6 octahedra of (a) $SrTiO_3$ (perovskite structure, cubic, $a = 0.3905$ nm) and (b) TiO_2 (anatase, tetragonal, $a = 0.3785$ nm, $c = 0.9513$ nm). (c) Schematic energy diagram of Ti $3d$-t_{2g} orbitals. Because TiO_6 for $SrTiO_3$ is a regular octahedra (left), the Ti $3d$-t_{2g} orbitals of $3d_{xy}$, $3d_{yz}$, and $3d_{zx}$ are located at the same energy level. On the contrary, that for anatase TiO_2 is irregularly shaped (right) and the $3d_{xy}$ orbital is at a lower energy level compared to $3d_{yz}$ and $3d_{zx}$ due to crystal field splitting.

[a)]Author to whom correspondence should be addressed; electronic mail: koumoto@apchem.nagoya-u.ac.jp

responding Ti 3*d* orbitals. Because TiO_6 in $SrTiO_3$ is a regular octahedra, the Ti 3*d*-t_{2g} orbitals of $3d_{xy}$, $3d_{yz}$, and $3d_{zx}$ are located at the same energy level [Fig. 1(c)]. On the contrary, TiO_2 is irregularly shaped. Thus, the $3d_{xy}$ orbital is located at a lower energy level compared to the $3d_{yz}$ and $3d_{zx}$ orbitals due to crystal field splitting.[11,12] Because the Seebeck coefficient reflects the density of states (DOS) of the bottom of the conduction band, comparing the carrier generation and transport properties such as n_e, m^*, and carrier relaxation time between $SrTiO_3$ and anatase TiO_2 will be beneficial for establishing future TE material selection and/or design concepts for Ti-based oxides. Herein we report the carrier generation and transport properties of high-quality epitaxial films of Nb-doped anatase TiO_2, which were grown by a pulsed-laser deposition (PLD) method, at high temperatures (300–900 K).

Nb-doped anatase TiO_2 films were heteroepitaxially grown on the (100)-face of $LaAlO_3$ single-crystalline substrates by PLD[13–16] with a KrF excimer laser ($\lambda = 248$ nm, pulse duration=20 ns, and repetition frequency=10 Hz) using polycrystalline rutile TiO_2 ceramic targets, which contained up to 30% Nb as a dopant, at a substrate temperature of 800 °C under flowing oxygen gas (oxygen partial pressure: 5.0×10^{-3} Pa). The crystalline quality, orientation, and thickness of the films were evaluated by high-resolution x-ray diffraction (HR-XRD) (ATX-G, Cu $K\alpha_1$, Rigaku Co.). The geometry of our x-ray diffractometer is described elsewhere.[17,18] The surface morphology of the films was observed by atomic force microscopy (AFM) (SPI-3800N, S.I.I) at room temperature. The optical absorption spectra were measured using both a UV-visible spectrometer (V-570, JASCO) and a Fourier transform infrared (FTIR) spectrometer (FT/IR-610, JASCO). The electrical conductivity (σ), carrier concentration (n_e), and Hall mobility (μ_{Hall}) of the films were measured by the dc four-probe method in the van der Pauw electrode configuration. The Seebeck coefficient (S) of the films was measured by a conventional steady-state method.

Figure 2(a) shows the out-of-plane HR-XRD pattern of a 20%-Nb-doped anatase TiO_2 film grown on the (100)-face of a $LaAlO_3$ substrate by PLD. Only intense Bragg diffraction peak of 004 anatase TiO_2 and 002 peak of the $LaAlO_3$ substrate are seen, indicating a mutual crystal orientation relationship of anatase $TiO_2(001) \| LaAlO_3(001)$. The lattice parameters of the anatase TiO_2 films were evaluated using reciprocal space mappings (RSMs) of the 028 diffraction spot from the 20%-Nb-doped anatase TiO_2 films, as shown in the inset. Although the lattice constant [Fig. 2(b)], c of the films proportionally increases with the Nb content, a significant Nb content dependence of a is not observed. Figure 2(c) shows a topographic AFM image of a 20%-Nb-doped anatase TiO_2 film. Atomically flat terraces and steps, which correspond to half the unit cell height of the anatase TiO_2 lattice, are clearly seen. These results indicate that heavily Nb-doped anatase TiO_2 epitaxial films with a high crystal quality are successfully fabricated on the (100)-face of a $LaAlO_3$ substrate.

Figure 3 shows typical optical absorption spectra of the Nb-doped anatase TiO_2 films at room temperature. The film

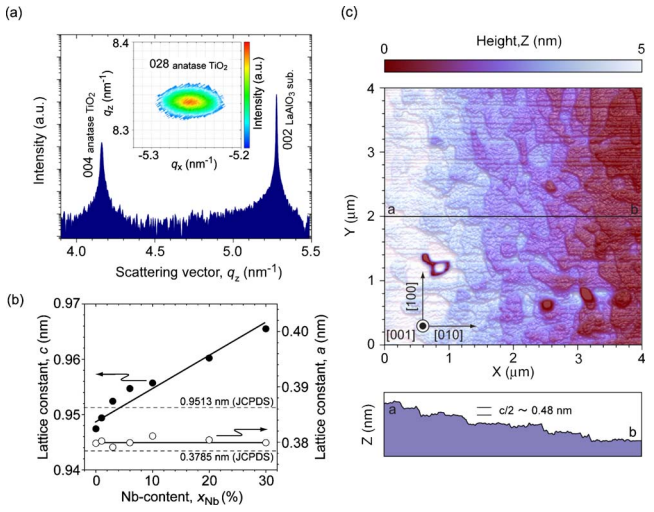

FIG. 2. (Color online) (a) Out-of-plane x-ray Bragg diffraction pattern of the 20%-Nb-doped anatase TiO_2 film. Intense peak of 004 anatase is seen along with 002 peak of the substrate. The inset shows reciprocal space mapping of the 028 diffraction spot of anatase TiO_2. (b) Lattice parameters (a and c axes) of several Nb-doped anatase TiO_2 epitaxial films. Values of TiO_2 powder[10] are also shown (dotted lines). (c) A topographic AFM image of a 20%-Nb-doped anatase TiO_2 film. Cross sectional profile from a to b is shown at the bottom.

changes from almost colorless to transparent blue as the Nb content increases. The UV-absorption edge, which is due to the direct bandgap of anatase TiO_2, is seen near 3.2 eV. This absorption edge gradually shifts to the higher energy side as the Nb content increases. In addition, intense absorption bands, which are probably due to the free electrons, are seen in the near infrared region. As shown in the inset, the optical bandgap (E_{gOPT}), which is evaluated by the $(\alpha h\nu)^2$-$h\nu$ plots of the UV-absorption edge for the anatase TiO_2 films, is plotted versus Nb content. The Burstein-Moss shift,[19–21] which is due to conduction band filling by carrier electrons, is clearly

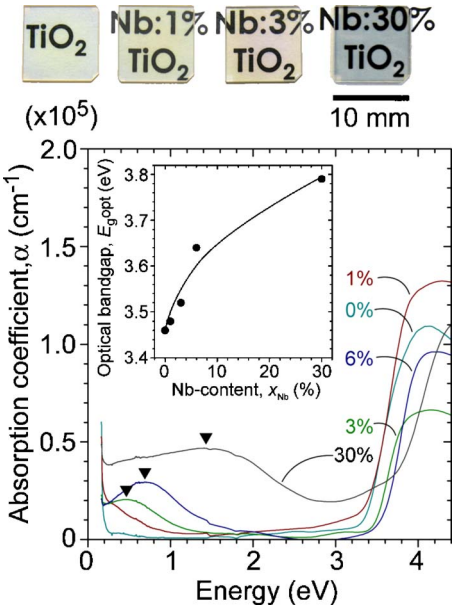

FIG. 3. (Color online) Optical absorption spectra of several Nb-doped anatase TiO_2 epitaxial films. The inset shows plots of Nb content, x_{Nb} vs optical bandgap, E_{gOPT}. (top) Photographs of several Nb-doped anatase TiO_2 films (thickness ~150 nm).

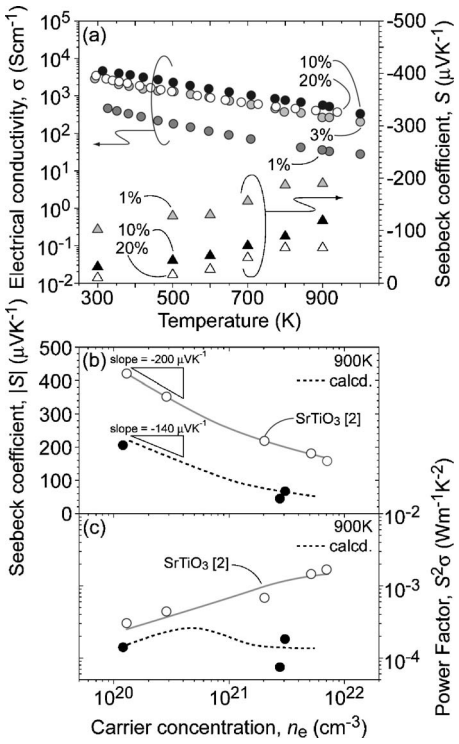

FIG. 4. (a) Temperature dependence of the electrical conductivity (σ) and Seebeck coefficient (S) for several Nb-doped anatase TiO_2 films. (b) Relationships between the carrier concentration (n_e) and $|S|$ for Nb-doped anatase TiO_2 and Nb-doped $SrTiO_3$ films at 900 K. (c) Relationships between n_e and the power factor ($S^2\sigma$) for Nb-doped anatase TiO_2 and Nb-doped $SrTiO_3$ films at 900 K.

seen, suggesting that doped Nb^{5+} ions act as the dopant.

Figure 4(a) shows the temperature dependence of the electrical conductivity (σ) and Seebeck coefficient (S) for the Nb-doped anatase TiO_2 epitaxial films. The S values are always negative, indicating that Nb-doped anatase TiO_2 epitaxial films are n-type semiconductors. In all cases, the σ value gradually decreases as the temperature increases. The Hall voltage measurements reveal that the anatase TiO_2 films are degenerate semiconductors and that the Hall mobility (μ_{Hall}) proportionally decreases with $T^{-2.5}$, which is most likely because polar optical phonon scattering is a dominant carrier scattering. The observed carrier concentration of the anatase TiO_2 films almost corresponds to the Nb content of the TiO_2 ceramic targets, e.g., 7.3×10^{21} cm^{-3} for 30%-Nb-doped anatase TiO_2. The $|S|$ values gradually increase as the temperature increases due to the fact that the chemical potential of a degenerate semiconductor gradually decreases as the temperature increases. It should be noted that the m^* value of anatase TiO_2 is $\sim1m_0$, which was evaluated using the values of n_e and S, and is an order of magnitude smaller than that of Nb-doped $SrTiO_3$ ($\sim10m_0$).[2]

Finally, we analyzed the $\log n_e$ dependence of the $|S|$ values[22] for the Nb-doped anatase TiO_2 epitaxial films at 900 K [Fig. 4(b)] to clarify the difference in the TE properties between Nb-doped anatase TiO_2 and Nb-doped $SrTiO_3$ at high temperature. The $|S|$ value gradually decreases as the $\log n_e$ increases. The slope of the $\log n_e$-$|S|$ plots for Nb-doped $SrTiO_3$ is approximately -200 μV K^{-1}, which is reasonable considering that the bottom of the conduction band is parabolic and the slope for TiO_2 is approximately -140 μV K^{-1}. The estimated thermoelectric power factor ($S^2\sigma$) of a $\sim$2%-Nb-doped anatase TiO_2 film ($n_e\sim5\times10^{20}$ cm^{-3}) is $\sim2.5\times10^{-4}$ W m^{-1} K^{-2} at 900 K [Fig. 4(c)], which is smaller than that of 20%-Nb-doped $SrTiO_3$ (1.5×10^{-3} W m^{-1} K^{-2}). From these results, we conclude that both m^* and DOS are reduced by the crystal field splitting of the Ti $3d$-t_{2g} orbitals. Thus, a Ti-containing metal oxide with a highly symmetrical structure should exhibit a better TE performance than a lower symmetrical one.

The carrier generation and transport properties of heavily Nb-doped anatase TiO_2 epitaxial films were measured at high temperatures (300–900 K). The carrier generation behavior and transport properties of the Nb-doped anatase TiO_2 epitaxial films were basically similar to those of Nb-doped $SrTiO_3$, except that the carrier effective mass (m^*) of the TiO_2 epitaxial films ($\sim1m_0$) was an order of magnitude smaller than that of Nb-doped $SrTiO_3$ ($\sim10m_0$). The estimated thermoelectric power factor ($S^2\sigma$) of a $\sim$2%-Nb-doped anatase TiO_2 film ($n_e\sim5\times10^{20}$ cm^{-3}) was $\sim2.5\times10^{-4}$ W m^{-1} K^{-2} at 900 K, which was smaller than that of a 20%-Nb-doped $SrTiO_3$ (1.5×10^{-3} W m^{-1} K^{-2}).

The present results demonstrate that cubic perovskite with a highly symmetrical structure exhibits a better TE performance than a tetragonal anatase with a low symmetrical structure. This information will help establish future TE material selection and/or design concepts for Ti-based metal oxides.

[1] T. M. Tritt *et al.*, in *Harvesting Energy Through Thermoelectrics: Power Generation and Cooling*, special issue of MRS Bull. 31, 188 (2006) and references therein.
[2] S. Ohta, T. Nomura, H. Ohta, M. Hirano, H. Hosono, and K. Koumoto, Appl. Phys. Lett. **87**, 092108 (2005).
[3] S. Ohta, T. Nomura, H. Ohta, and K. Koumoto, J. Appl. Phys. **97**, 034106 (2005).
[4] T. Okuda, K. Nakanishi, S. Miyasaka, and Y. Tokura, Phys. Rev. B **63**, 113104 (2001).
[5] I. Terasaki, Y. Sasago, and K. Uchinokura, Phys. Rev. B **56**, R12685 (1997).
[6] M. Shikano and R. Funahashi, Appl. Phys. Lett. **82**, 1851 (2003).
[7] B. A. Cook, J. L. Harringa, S. H. Hann, and C. B. Vining, J. Appl. Phys. **78**, 5474 (1995).
[8] I. Nishida, Phys. Rev. B **7**, 2710 (1973).
[9] JCPDS Card No. 05-0634.
[10] JCPDS Card No. 21-1272 .
[11] R. Asahi, Y. Taga, W. Mannstadt, and A. J. Freeman, Phys. Rev. B **61**, 7459 (2000).
[12] N. Daude, C. Gout, and C. Jouanin, Phys. Rev. B **15**, 3229 (1977).
[13] Y. Matsumoto *et al.*, Science **291**, 854 (2001).
[14] Y. Furubayashi, T. Hitosugi, Y. Yamamoto, K. Inaba, G. Kinoda, Y. Hirose, T. Shimada, and T. Hasegawa, Appl. Phys. Lett. **86**, 252101 (2005).
[15] Y. Furubayashi, T. Hitosugi, Y. Yamamoto, Y. Hirose, G. Kinoda, K. Inaba, T. Shimada, and T. Hasegawa, Thin Solid Films **496**, 157 (2006).
[16] M. Murakami *et al.*, Appl. Phys. Lett. **78**, 2664 (2001).
[17] H. Ohta, K. Nomura, M. Orita, M. Hirano, K. Ueda, T. Suzuki, Y. Ikuhara, and H. Hosono, Adv. Funct. Mater. **13**, 139 (2003).
[18] K. Nomura *et al.*, J. Appl. Phys. **95**, 5532 (2004).
[19] Y. Ohhata, F. Shinoki, and S. Yoshida, Thin Solid Films **59**, 255 (1979).
[20] E. Burstein, Phys. Rev. **93**, 632 (1954).
[21] T. S. Moss, Proc. Phys. Soc. London, Sect. B **67**, 775 (1954).
[22] G. H. Jonker, Philips Res. Rep. **23**, 131 (1968).